Seventh International Conference on
Computational Fluid Dynamics (ICCFD7),
Big Island, Hawaii, July 9-13, 2012

ICCFD7-4302

Characterization and Design of Tubercle Leading-Edge Wings

Mark W. Lohry, David Clifton and Luigi Martinelli
Corresponding author: mlohry@princeton.edu

Department of Mechanical and Aerospace Engineering
Princeton University, Princeton, NJ 08544, USA

Abstract: Leading-edge wing planform variations modeled after protuberances seen on humpback whale flippers are believed to result in improved lift and drag characteristics in the near-stall regime. The unconventional geometry makes flow predictions highly sensitive to turbulence models which are otherwise well validated for conventional wings at high Reynolds numbers. We carry out a computational study aimed at validating a RANS approach for the analysis of tubercles in a Reynolds number range 62,500 - 500,000. Comparisons with experimental observations are presented and the relevant flow physics are discussed.

Keywords: CFD, Turbulence Modeling, Unsteady Flows, High Lift Devices.

1   Introduction

Since the 2004 paper by Miklosovic, Murray, Howle and Fish [1], there has been a growing body of empirical evidence which demonstrates potential benefits of the so-called tubercular leading edge wings. Tubercles are bio-inspired aerodynamic devices that originate from the morphology of the humpback (*Magaptera novaeangliae*) whale flipper, whose appearance resemble knuckles extruding out of the wing leading edge. The humpback is known for performing tight turning maneuvers, and biologists have inferred that tubercles are responsible for the generation of the necessary aerodynamic forces. Since the radius of curvature of the maneuver is inversely proportional to the lift, one should conclude that tubercles might contribute to the increased maximum lift.

Stall delay and stall mitigation appear to be achievable by properly placing tubercles on the leading edge of a wing and it is believed that the the physical mechanism controlling the observed stall mitigation involves the generation of stream-wise vorticity which energizes the viscous layer. From this point of view, optimizing tubercle shape and placement would be equivalent to the problem of optimizing vortex generators by using CFD, which is *per se* a challenging computational problem, but CFD analysis of tubercular wings presents additional complications.

One source of difficulties is that wing planform and span-loading play a significant role in determining the aerodynamic performance of the tubercles, and the tubercles' size and distribution should be tailored to a given wing planform and span-wise load distribution. Van Nierop et al [2] attempted to analyze these issues by using Prandtl lifting line approach, an inviscid theory which cannot account directly for the viscous phenomena controlling separation and stall. On a fully three dimensional wing, tubercles may actually act as fences and decrease the span-wise flow, and depending on the location and span loading they could be particularly efficient on delaying the outboard stall. This is strongly suggested by the results of several CFD studies, including our own, which utilize a whale flipper planform [3]. In order to properly understand the flow physics and the shape parameters controlling the efficiency of the tubercles, it is therefore advisable to try to decouple the planform from the tubercle shapes. This has indeed been done experimentally by Miklosovic et al [4], Hansen et al [5] and Johari et al [6] but we are not aware of any extensive CFD analysis performed on these simpler configurations.

One additional complication is that there also exists empirical evidence suggesting that tubercles might actually be detrimental. As it was noted by Hansen et al [5] it appears that the studies showing negative effects are at a Reynolds number less than 300,000, while those showing benefits are generally at Reynolds number greater than 500,000. This strong dependence on Reynolds number can be a challenge for RANS methods which are generally not well calibrated for low Reynolds number, potentially transitional flow.

For these reasons, although the ultimate goal of our study is to use shape optimization tools of the class developed at Princeton by Jameson, Martinelli and Pierce [7] to determine optimal shapes of tubercled wings, we found it necessary to preface the optimization study by a careful CFD analysis of this class of flow. The results of this study are the subject of this paper.

Most of the experimental data available for validation are for low Reynolds numbers, in the range 120,000 - 270,000. This is a difficult regime for RANS solvers because of the uncertainties related to the performance of turbulence models in transitional regimes, and the ability of RANS solvers to properly capture laminar separation bubbles which might be present. In the present work, we use the experimental study of Miklosovic [4] for validation and we attempt to characterize the effects of geometry parameters by analyzing the flow separation patterns leading to stall of several tubercular wings with a sinusoidal planform.

A finite volume method developed at Princeton over the past two decades, one that is well validated for high Reynolds number flows, is employed. The multigrid iterative scheme allows one to compute a steady calculation of this size with modest computational resources. When coupled with an appropriate backward difference formula (BDF), it is feasible to compute the time dependent stall and post stall regimes on meshes with 15-25 million cells. Although our numerical method is well documented in the literature it will be briefly reviewed in the following section.

2   Numerical Method

The discretization of the spatial operators is accomplished by using a finite volume method to the integral form of the RANS equations. Both cell centered and vertex based schemes [8] have been developed in our group at Princeton over a period of ten years from 1985-1995; a cell centered formulation was used for this study. The convective fluxes are computed using the integral form of the conservation laws, which has the advantage that no assumption of the differentiability of the solution is implied. In general the control volumes could be arbitrary, but in this work we use the hexahedral cells of a body-conforming curvilinear mesh. To include the viscous terms of the Navier-Stokes equations into the spatial discretization scheme it is necessary to approximate the velocity derivatives $\frac{\partial u_i}{\partial x_j}$, which constitute the stress tensor σ_{ij}. These derivatives are evaluated by applying Gauss' formula to a control volume V with boundary S:

$$\int_V \frac{\partial u_i}{\partial x_j} dV = \int_S u_i n_j dS \ ,$$

where n_j is the outward normal. For a hexahedral cell this gives

$$\overline{\frac{\partial u_i}{\partial x_j}} = \frac{1}{V} \sum_{\text{faces}} \ \overline{u}_i \ n_j \ S \ , \tag{1}$$

where $\overline{u}_i$ is an estimate of the average of u_i over the face, n_j is the jth component of the normal, and S is the face area. Very efficient, low storage implementations of this formula were developed, in which one can store only two planes of data.

Discretizations of this type reduce to central differences on a regular Cartesian grid, and in order to eliminate possible odd-even decoupling modes allowed by the discretization of the convective terms some form of background artificial dissipation must be added.

The effects of numerical diffusion, which may be introduced either explicitly to avoid decoupling or implicitly by means of upwind formulas, could adversely impact the overall accuracy of the solution. Thus, extreme care in devising an appropriate numerical diffusion or upwind method is required.[9] Several dissipation schemes have been developed and thoughruly validated for viscous flow [10]; we refer the interested reader to the available literature [11, 12].

When the space discretization procedure is implemented separately from the discretization in time, it leads to a set of coupled ordinary differential equations which can be written in the form

$$\frac{d\mathbf{w}}{dt} + \mathbf{R}(\mathbf{w}) = \mathbf{0}, \tag{2}$$

where $\mathbf{w}$ is the vector of the flow variables at the mesh locations, and $\mathbf{R}(\mathbf{w})$ is the vector of the residuals, consisting of the flux balances defined by the spatial discretization together with the added dissipative terms. If the objective is simply to reach the steady state and details of the transient solution are immaterial, the time-stepping scheme may be designed solely to maximize the rate of convergence. For steady flow multigrid acceleration is applied to a multistage time-stepping scheme, which yields rapid convergence to a steady state even for the large meshes used in this study. The explicit nature of the multigrid time-stepping scheme makes it suitable for efficient implementation on parallel computers.[13, 14]

The parallelization strategy of choice developed in collaboration with J. Alonso [15, 16] uses a domain decomposition model, a SPMD (Single Program Multiple Data) approach, and the MPI (Message Passing Interface) library for message passing. The resulting codes are readily portable to different parallel computing platforms as well as to homogeneous and heterogeneous networks of workstations.

Communication between subdomains is performed through halo cells surrounding each subdomain boundary. Since both the convective and the viscous fluxes are calculated at the cell faces (boundaries of the control volumes), all six neighboring cells are necessary, thus requiring the existence of a single level halo for each processor in the parallel calculation. The calculation of the dissipative fluxes requires values from the twelve neighboring cells (two adjacent to each face). For each processor, some of these cells will lie directly next to an interprocessor boundary, in which case the values of the flow variables residing in a different processor will be necessary to calculate the fluxes. The actual communication routines used are all of the asynchronous (or non-blocking) type.

2.1 BDF scheme for time accurate flow

In the stall and post-stall regime, time accurate calculations need to be performed to account for the unsteadiness of flow filed. In this regime we used an implicit, dual time-stepping multigrid approach. The idea, first put forth by Jameson in 1991 [17] and extended to the RANS equations by Alonso and Martinelli [18], is to use an implicit scheme with a large stability region (A-stable or stiffly stable) and to solve the implicit equations at each time step by inner iterations using an accelerated time evolution scheme in artificial time. The second order BDF is

$$\frac{3}{2\Delta t} w^{n+1} - \frac{2}{\Delta t} w^n + \frac{1}{2\Delta t} w^{n-1} + R(w^{n+1}) = 0. \tag{3}$$

With a dual time stepping one solves

$$\frac{dw}{dt^*} + \frac{3}{2\Delta t} w - \frac{2}{\Delta t} w^n + \frac{1}{2\Delta t} w^{n-1} + R(w) = 0 \tag{4}$$

in pseudo time t^* to reach a steady state satisfying equation (3). This construction of an implicit scheme allows one to use fast steady state solvers, such as the multigrid time-stepping used for our steady calculations, while maintaining all the advantages of an implicit method. This approach has been successfully validated for computing time-dependent compressible [18] and incompressible viscous flow [19].

3 Validation Study

As it was mentioned in the introduction, predictions using RANS in the Reynolds number of interest is particularly difficult. Moreover, in order to understand the flow physics controlling the performance of tubercles, we chose to decouple the effects of span loading from the effects attributable solely to the tubercle geometry. In decoupling planform effects from that of the tubercles, the experimental work by Miklosovic et al [18] compared a straight wing with a NACA0020 airfoil to a sinusoidally varying tubercle geometry based on the NACA0020, and we chose to use this geometry as a baseline.

3.1 Wing Geometry

For the tubercled wing, the leading edge of the planform is given by

$$x_{LE} = 0.04 \cos(4.878\pi z) \qquad (5)$$

where z is the coordinate along the span. To create the tubercles, the cross-section is modified by a non-linear shearing transformation that maintains the leading edge radius, the position of maximum thickness, and the airfoil shape behind that point [20].

$$d\eta' = \begin{cases} (1 + B\sin\pi\eta)d\eta & \forall \quad \eta < 0.3 \\ d\eta & \forall \quad \eta \geq 0.3 \end{cases} \qquad (6)$$

$$\eta = \frac{x_0 - x_{LE}}{C'} \qquad \eta' = \frac{x' - x_{LE}}{C'} \qquad B = k_0\left(\frac{C'}{C_0} - 1\right)$$

where x_0 is the unscaled NACA0020 coordinate, $C' \equiv x_{TE} - x_{LE}$ is the local scaled chord length determined by the given leading edge variation 5, and C_0 is the unmodified chord length, taken throughout this work as 1. Integrating equation 6 gives

$$\eta' = \begin{cases} \eta - \frac{B}{\pi}\cos\pi\eta + k_1 & \forall \quad \eta < 0.3 \\ \eta & \forall \quad \eta \geq 0.3 \end{cases} \qquad (7)$$

For the $\eta < 0.3$ case the scaled coordinate is then

$$x' = x_0 - C'\frac{k}{\pi}(C'/C_0 - 1)\cos\pi\frac{x_0 - x_{LE}}{C'} + k_1 \qquad (8)$$

where the integration constant k_1 can be found from the condition that the modified leading edge point x_{LE} corresponds to the leading edge point $x_{0,LE}$ of the unmodified section where $\eta' = 0$,

$$k_1 = x_{LE} - x_{0,LE} + \frac{k_0}{\pi}\left(\frac{C'}{C_0} - 1\right)C'\cos\left(\pi\frac{x_{0,LE} - x_{LE}}{C'}\right) \qquad (9)$$

The k_0 term can be determined by requiring a smooth transition at $\eta = \eta' = 0.3$,

$$k_1 = \frac{k_0}{\pi}\left(\frac{C'}{C_0} - 1\right)\cos 0.3\pi \rightarrow$$

$$k_0 = \frac{x_{0,LE} - x_{LE}}{\frac{C'/C_0 - 1}{\pi}\left[C'\cos\left(\pi\frac{x_{0,LE} - x_{LE}}{C'}\right) - \cos 0.3\pi\right]} \qquad (10)$$

The cross-section that results from this transformation can be seen in figure 1.

    In order to begin characterizing the design space for these unconventional wings, we also test another variation defined by maintaining straight leading and trailing edges and scaling only the thickness of the cross-section by the same sinusoidal variation. This has the effect of creating smooth channels in the flow direction. Side views of the geometries can be seen in figure 1.
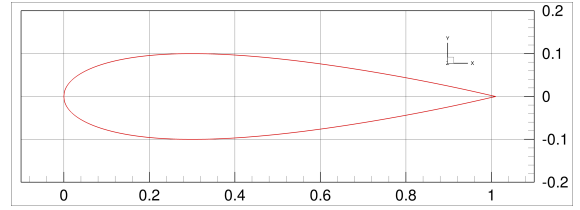
(a) Straight NACA0020 section.
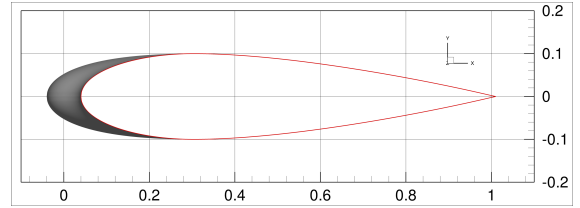
(b) Tubercle wing cross-section.
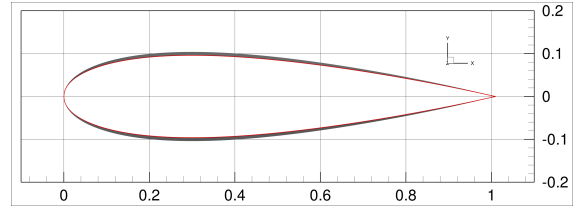
(c) Channel wing cross-section.
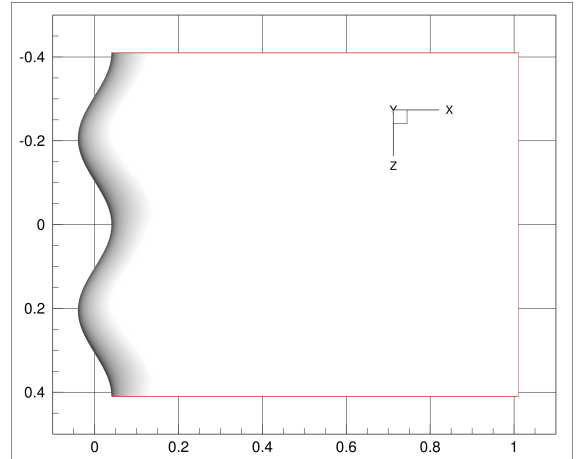
(d) Tubercle wing planform.

Figure 1: Wing geometries.

3.2 Meshing and Computation

All geometries tested here were meshed with a single C-block consisting of 16.7 million cells created by hyperbolic extrusion from the wing surface. The surface meshes have 128 faces on each side of the chord in the streamwise direction and 256 in the spanwise direction. For conventional wings fewer cells are typically used, resulting in higher aspect ratio cells near the body, which gives acceptable accuracy as the typical gradients in the spanwise and streamwise directions are very small compared to those normal to the body. The geometries of interest here naturally create significant flow variations in the spanwise and streamwise directions, requiring much denser surface meshes. Convergence rates and accuracy for ~ 5 million cell grids were generally poor; Weber et al [3] previously noted a 10% change in C_L in refining from 1.4 to 2.3 million cells on the similar three-dimensional finite wing case.

For the non-straight wings, two full periods of the variation were meshed in order to capture possible larger scale flow features, with periodic boundary conditions applied in the spanwise direction. The first grid point was placed at 4.37×10^{-5} chord lengths from the wing surface, giving the first cell-centered solution node at $y^+ = 0.5$ for a $Re = 500,000$ flow. The same grids are used for the less restrictive $Re = 275,000$ simulations, which constitute the bulk of this work. Since a primary goal of the simulations is the accurate prediction of separation and near-wall flow behavior that affect stall, this resolution was chosen to eliminate the need to use wall functions in the RANS solution. The two equation SST (shear stress transport) $k - \omega$ turbulence model of Menter was used, which is noted to produce good results in separated flows and can be used without a wall model [21, 22]. All simulations were performed at $M_\infty = 0.1$.

Princeton's *Della* research computing cluster was used for the simulations. It is comprised of 128 compute nodes with 12 2.67GHz Intel Westmere CPU cores on each node. Simulations below $\alpha = 10°$ were run in steady mode, requiring 72 CPU-hours to converge. Above $\alpha = 10°$ unsteady features started to emerge, necessitating time-accurate simulations which typically converged to a statistically steady state in 192-240 CPU-hours. Most calculations were run on a single node using 6 or 12 cores and required between 12 and 20 hours wall-time. This scaling is linear with the number of iterations required. Additionally, parallel performance of the code scales almost linearly with the number of cores used.

3.3 Results

Figures 2(a) and 2(b) show a comparison of the results obtained for all the configurations of this study and include the experimental data available for the two of them - the straight leading edge baseline wing and the sinusoidal tubercle shaped by the shearing transformation discussed in the previous section. A comparison with the results obtained for the baseline wing with a Spalart-Allmaras (blue circles) and Menter SST (red circles) indicates that the SST model reproduces more closely the experimental curves, and therefore was selected for the remainder of this study. Overall the trend and the magnitude of the computed lift and drag compare favorably with the experimental observation, with the exception of two data points in the post stall regime. The evolution of the turbulent intensity field and the velocity profiles are presented next for future comparison.
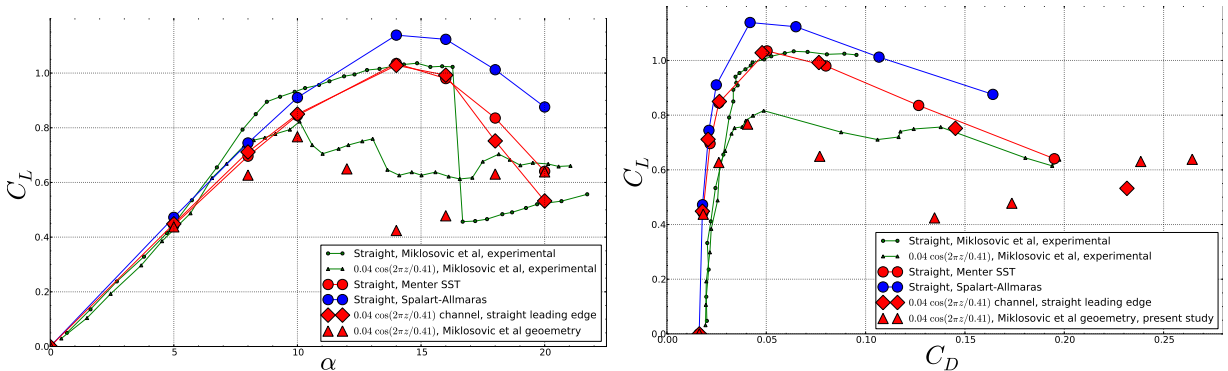
Figure 2: Lift curve and drag polar for tested geometries. Experimental data from Miklosovic et al.[1]
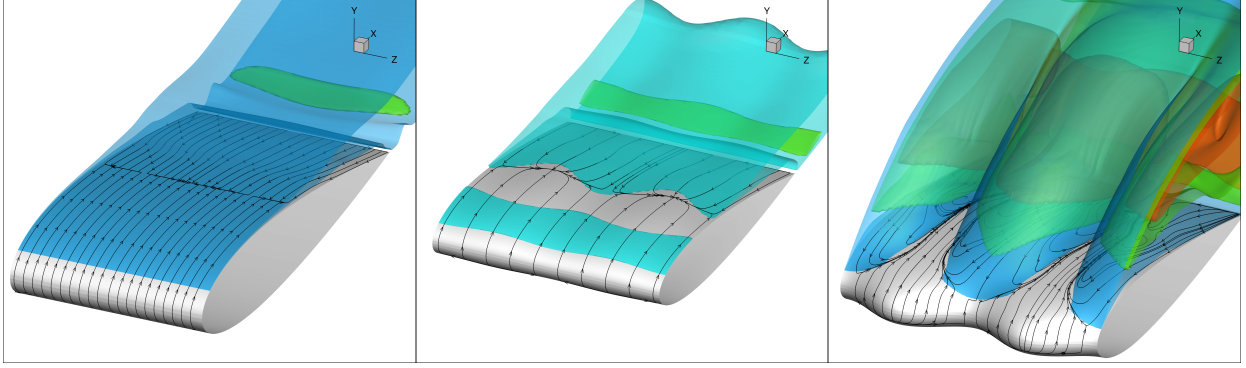
Figure 3: Isosurfaces of turbulent kinetic energy for straight, channel, and tubercled wing at $\alpha = 14°$. Note the sharp increase in turbulent energy at the separation lines.

3.4   Separation Patterns

The stall and post-stall characteristics are dominated by large regions of flow separation. Three-dimensional separation is generally an abrupt phenomenon which is difficult to describe, let alone understand, without a precise framework. To assimilate the computed results on the separation patterns of the configurations considered in this study, we find a critical point analysis to be most useful. This techniques was first proposed by Robert Legendre in the 1950's and adopted by Lighthill in 1963 [23].

Separation is described by analogy to a dynamical analysis of autonomous systems. If one recognizes that in a steady flow the streamlines next to the wall obey, and hence the skin-friction lines obey, on a surface $\eta = \text{constant}$ described by a local $\eta - \xi - \zeta$ coordinate system, the equations:

$$\frac{d\xi}{\tau_\xi(\xi,\zeta)} = \frac{d\zeta}{\tau_\zeta(\xi,\zeta)}.$$

To study the shape of the skin friction lines in the vicinity of a singular point

$$\tau_\xi = \tau_\zeta = 0$$

the solution can be expanded locally in a Taylor series, which leads to an eigenvalue problem for the Jacobian

$$J = \left| \begin{array}{cc} \frac{\partial \tau_\xi}{\partial \xi} & \frac{\partial \tau_\zeta}{\partial \xi} \\ \frac{\partial \tau_\xi}{\partial \zeta} & \frac{\partial \tau_\zeta}{\partial \zeta} \end{array} \right| ,$$

and the behavior of the skin friction lines in the vicinity of the critical point is determined by eigenvalues of J. From this consideration the analogy with the critical point analysis of an autonomous system becomes self evident.

Separation and reattachment patterns are then described uniquely in term of stable and unstable nodes, saddle points, as well as stable and unstable foci. The excellent reviews by Tobak and Peake [24] and Delery [25] provide comprehensive historical background on the subject, here we just make use of this formalism to describe our results.

The skin friction for the straight wing, channel wing, and tubercle wing are compared in figure 5. It can be noticed that the effect of the channel is to create two well defined separation nodes which leads to a break-up of the separation region in two separate zones, while the presence of the tubercle leads to a richer separation pattern, with multiple foci representing vortices shedding from the surface.

These characteristics appears to be more pronounced and effective at a higher Reynolds number, as illustrated in figure 7.

From this analysis, it can be concluded that both thickness variation and planform shaping should be used in designing an effective tubercle. Also, our results indicates that the ultimate performance of tubercles are indeed dependent on Reynolds number, at least in the range considered here. To validate our method

(c) Velocity profile, peak.

(d) Velocity profile, peak.

(e) Velocity profile, trough.

(f) Velocity profile, trough.

(g) Turbulence intensity, peak.

(h) Turbulence intensity, peak.

(i) Turbulence intensity, trough.

(j) Turbulence intensity, trough.
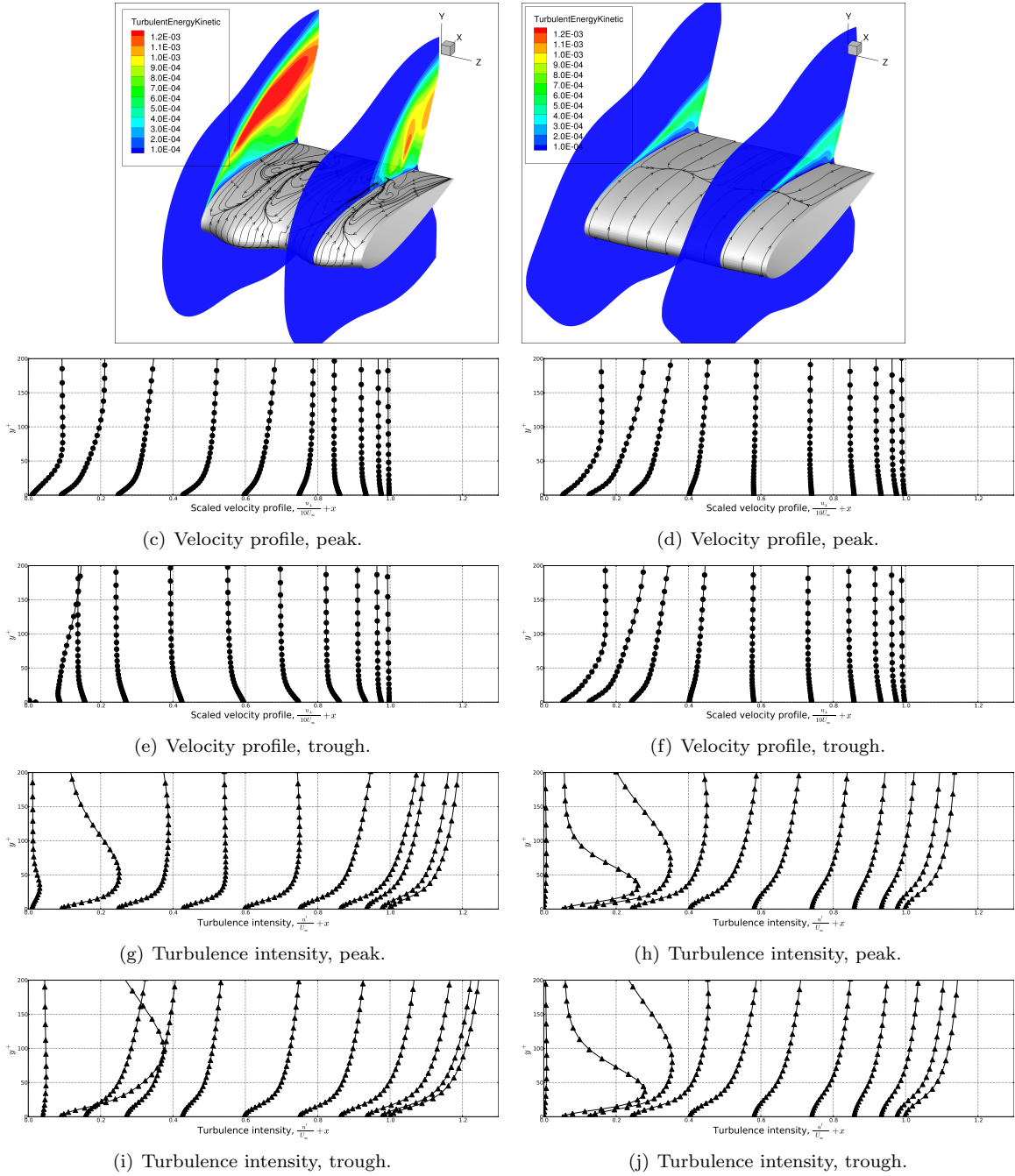
Figure 4: Boundary layer profiles for tubercled (left) and channel (right) wings at $\alpha = 14°$.
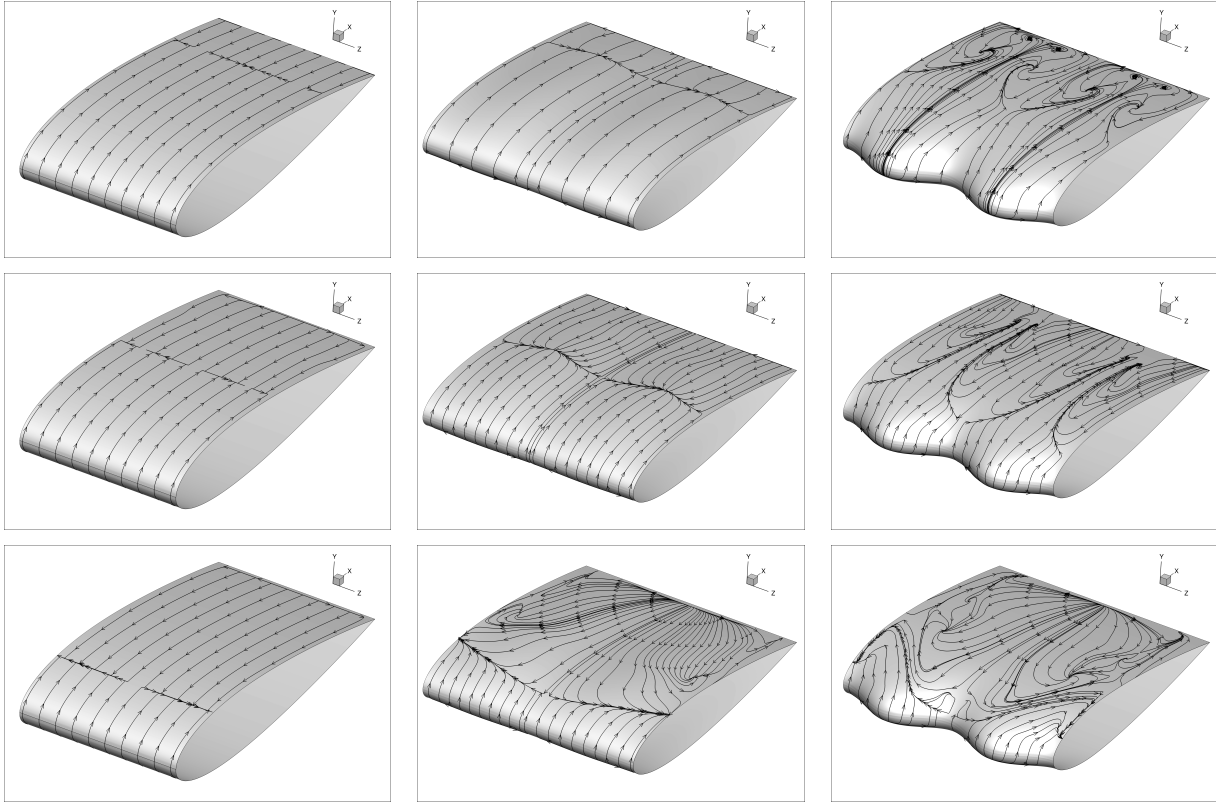
Figure 5: Surface oil flow pattern for geometries from left to right: straight wing, channel wing, and tubercle wing, at $\alpha = 10°$, $14°$, and $18°$ from top to bottom.

on a full three-dimensional wing, we have computed the Miklosovic whale flipper model presented next.

3.5 Finite Span Wing

In order to validate the methods used for a fully three-dimensional wing, we have run calculations on the finite-span tubercular geometry from Miklosovic et al [1]. Our computed lift coefficient results compare well with the experimental data available for a Reynolds number of 500000 up to the stall region. The computed drag coefficient is slightly higher than the experiment, but is consistent with the computed results of Weber [3] for the same case, which were obtained using the commercial CFD solvers Star-CCM+ and SolidWorks Flow Simulation, and that of Pedro et al [26], which were obtained using Fluent. Both of these previous computations were performed using wall functions and coarser grids (approximately 2.5 million cells). Although in error, our drag calculations appear to be closer to experiment, most likely due to the higher resolution (6.5 million cells) used here. This suggests a more detailed grid refinement study for the three-dimensional case is needed.

4 Conclusion

The efficiency of our solver allowed fast calculations of steady and unsteady flow on well resolved meshes with modest computational resources. In the course of this study we found that CFD analysis using RANS closed by a Menter SST turbulence model reproduces experimental measurements and trends with reasonable accuracy, even at a Reynolds numbers lower than the one encountered in most envisioned practical applications. This makes shape optimization of wings with tubercles using an adjoint method feasible.

By interpreting the skin friction lines in the separation region in terms of critical points we were able to infer that tubercles built by chord variations and constant thickness act as vortex generators. On periodic
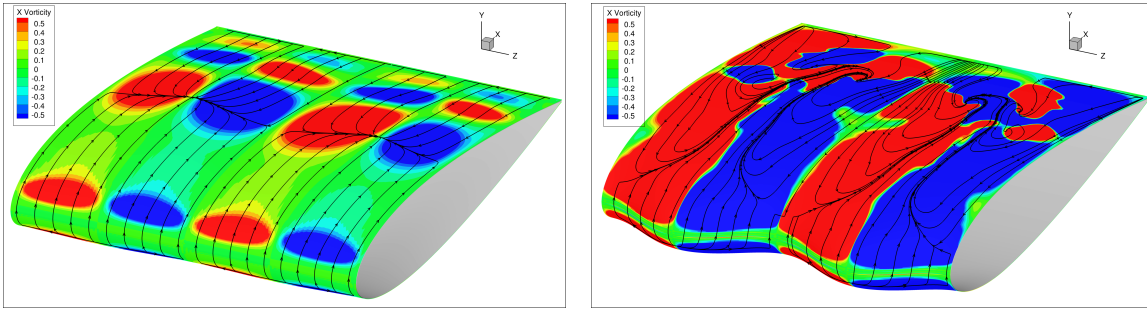
Figure 6: Near-surface streamwise vorticity for channel and sinusoidal wings at $\alpha = 14°$.
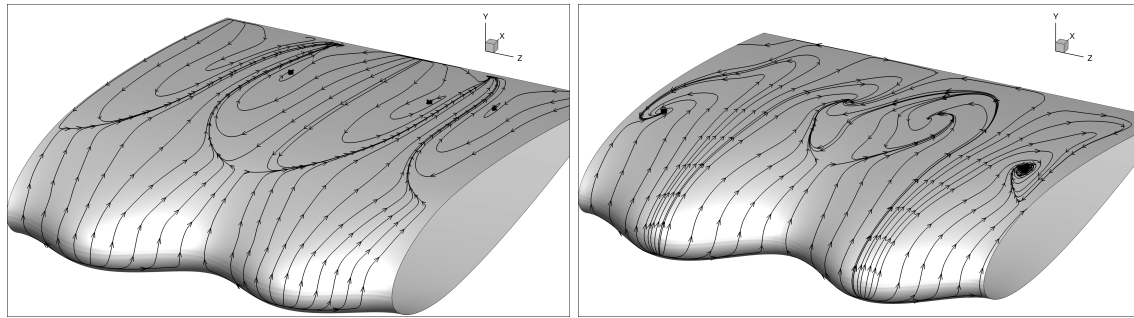
(a) $Re = 275,000$ (b) $Re = 500,000$

Figure 7: Surface oil flow pattern for tubercle wing at $\alpha = 12°$.

wings they tend to reduce $C_{l_{max}}$ but mitigate the stall, by sustaining higher levels of lift for higher angles of attack. Tubercles may be used successfully to energize the flow at critical span-wise locations, potentially improving the outboard stall characteristics as in the case of Miklosovic's whale flipper model. Our results confirm Hensen's observation that tubercles might be detrimental at low Reynolds numbers.

We have also shown that a variation in thickness along the span, which creates channels of sorts along the chord, can be used to break up the separation regions and create spanwise fences, which can increase $C_{l_{max}}$. Our observations indicate that a fully three-dimesional shape optimization is necessary to design tubercles with higher performance; this is the subject of our ongoing research. Also, recalling that the humpback is known for performing tight turn maneuvering, an in depth assessment of tubercle performance in dynamic stall conditions seems *de rigueur*.
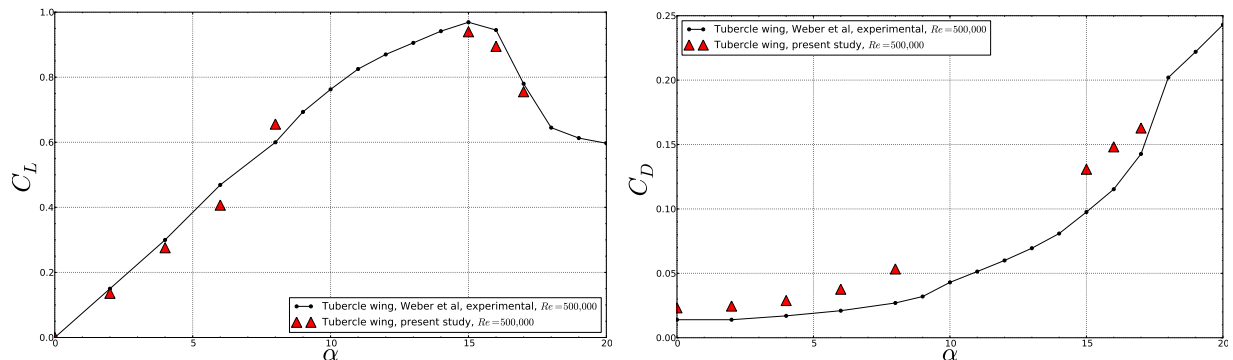
Figure 8: Lift and drag coefficients for smooth and tubercle wings. Experimental data from [3].

Acknowledgement

References

[1] D. S. Miklosovic, M. M. Murray, L. E. Howle, and F. E. Fish. Leading-edge tubercles delay stall on humpback whale (Megaptera novaeangliae) flippers. *Physics of Fluids*, 16(5):L39–L42, March 2004.

[2] Ernst A. van Nierop, Silas Alben, and Michael P. Brenner. How bumps on whale flippers delay stall: An aerodynamic model. *Physical Review Letters*, 100(5):054502, February 2008.

[3] Paul W. Weber, Laurens E. Howle, Mark M. Murray, and David S. Miklosovic. Computational evaluation of the performance of lifting surfaces with leading-edge protuberances. *Journal of Aircraft*, 48(2):591–600, 2011.

[4] D.S. Miklosovic, M.M. Murray, and L.E. Howle. Experimental evaluation of sinusoidal leading edges. *Journal of aircraft*, 44(4):1404–1408, 2007.

[5] Kristy L. Hansen, Richard M. Kelso, and Bassam B. Dally. Performance variations of leading-edge tubercles for distinct airfoil profiles. *Journal of Aircraft*, 49(1):185–194, 2011.

[6] H. Johari, C. Henoch, D. Custodio, and A. Levshin. Effects of leading-edge protuberances on airfoil performance. *AIAA Journal*, 45(11):2634–2642, 2007.

[7] A. Jameson, N. Pierce, and L. Martinelli. Optimum aerodynamic design using the Navier-Stokes equations. *AIAA paper 97-0101*, January 1997.

[8] L. Martinelli, A. Jameson, and E. Malfa. Numerical simulation of three-dimensional vortex flows over delta wing configurations. In M. Napolitano and F. Solbetta, editors, *Proc. 13th International Confrence on Numerical Methods in Fluid Dynamics*, pages 534–538, Rome, Italy, July 1992. Springer Verlag, 1993.

[9] S. Tatsumi, L. Martinelli, and A. Jameson. Design, implementation, and validation of flux limited schemes for the solution of the compressible navier-stokes equations. In *1994 32 nd AIAA Aerospace Sciences Meeting and Exhibit*, 1994.

[10] L. Martinelli and A. Jameson. Mesh refinement and modeling errors in flow simulations. *AIAA Journal*, 36:676–685, 1998.

[11] L. Martinelli and A. Jameson. Viscous flow solvers for aero/hydrodynamic analysis and design. *AIAA paper 98-3003*, AIAA 33rd Aerospace Sciences Meeting and Exhibit, Albuquerque, June 1998.

[12] J. Reuther, J. J. Alonso, J. C. Vassberg, A. Jameson, and L. Martinelli. An efficient multiblock method for aerodynamic analysis and design on distributed memory systems. *AIAA paper 97-1893*, June 1997.

[13] A. Jameson. Multigrid algorithms for compressible flow calculations. In W. Hackbusch and U. Trottenberg, editors, *Lecture Notes in Mathematics, Vol. 1228*, pages 166–201. Proceedings of the 2nd European Conference on Multigrid Methods, Cologne, 1985, Springer-Verlag, 1986.

[14] L. Martinelli and A. Jameson. Validation of a multigrid method for the Reynolds averaged equations. *AIAA paper 88-0414*, 1988.

[15] J. J. Alonso, T. J. Mitty, L. Martinelli, and A. Jameson. A two-dimensional multigrid Navier-Stokes solver for multiprocessor architectures. In Satofuka, Periaux, and Ecer, editors, *Parallel Computational Fluid Dynamics: New Algorithms and Applications*, pages 435–442, Kyoto, Japan, May 1994. Elsevier Science B. V. Parallel CFD '94 Conference.

[16] A. Jameson and J. J. Alonso. Automatic aerodynamic optimization on distributed memory architectures. *AIAA paper 96-0409*, AIAA 34th Aerospace Sciences Meeting and Exhibit, Reno, NV, January 1996.

[17] A. Jameson. Time dependent calculations using multigrid, with applications to unsteady flows past airfoils and wings. *AIAA paper 91-1596*, AIAA 10th Computational Fluid Dynamics Conference, Honolulu, Hawaii, June 1991.

[18] J. J. Alonso, L. Martinelli, and A. Jameson. Multigrid unsteady Navier-Stokes calculations with aeroelastic applications. AIAA paper 95-0048, AIAA 33rd Aerospace Sciences Meeting and Exhibit, Reno, NV, January 1995.

[19] A. Belov, L. Martinelli, and A. Jameson. A new implicit algorithm with multigrid for unsteady incompressible flow calculations. In *23rd AIAA Aerospace Sciences Meeting and Exhibit*, 1995.

[20] Paul W. Weber, Laurens E. Howle, and Mark M. Murray. Lift, drag, and cavitation onset on rudders with leading-edge tubercles. *Marine Technology*, 47(1):27–36, 2010.

[21] F. R. Menter. Zonal two-equation $k - \omega$ turbulence model for aerodynamic flows. In *AIAA Paper 93-2906*, 1993.

[22] Florian R. Menter. Review of the shear-stress transport turbulence model experience from an industrial perspective. *International Journal of Computational Fluid Dynamics*, 23(4):305–316, 2009.

[23] L. Rosenhead. *Laminar boundary layers: an account of the development, structure, and stability of laminar boundary layers in incompressible fluids, together with a description of the associated experimental techniques.* Clarendon press, 1963.

[24] M. Tobak and D. J. Peake. Topology of three-dimensional separated flows. *Annual Review of Fluid Mechanics*, 14:61–85, 1982.

[25] J.M. Délery. Robert legendre and henri werlé: toward the elucidation of three-dimensional separation. *Annual review of fluid mechanics*, 33(1):129–154, 2001.

[26] H.T.C. Pedro and M.H. Kobayashi. Numerical study of stall delay on humpback whale flippers. In *46th AIAA Aerospace Sciences Meeting and Exhibit*, pages 2008–0584, 2008.